Lasers in Manufacturing Conference 2021

Joining technology and mechanical properties of laser-beam welded joints with martensitic chromium steels

Martin Dahmen[a,]*, Jörg Baumgartner[b], Benjamin Möller[b],Viktoria Olfert[c,], Rainer Wagener[b]

[a]*Fraunhofer Institute for Laser Technology, Steinbachstrasse 15, 52074 Aachen, Germany*
[b]*Fraunhofer Institute for Structural Durability and System Reliability, Bartningstrasse 47, 64289 Darmstadt, Germany*
[c] *Laboratory for Material and Joining Technology, Paderborn University.Pohlweg 47-49, 33098 Paderborn, Germany*

Abstract

Investigations were undertaken on welding of press-hardened martensitic stainless steels in similar joints as well as in combination with state-of-the-art and modern steel grades. Parameter development was conducted for square-butt and lap joint configuration aiming at the production of defect-free welds. In order to homogenise the mechanical properties of the weld area, a heat treatment has been developed and applied successfully. Tests on load capacity of lap joints have been carried out under quasi-static and dynamic loading using the LWF-KS2 concept. Emphasis is laid on the investigation of contour welds. Especially for the chromium steel a strong dependence on the load angle was detected. Heat treatment led to a significant improvement of strength and ductility. Independent of heat treatment and seam weld shape, uni-directional fatigue testing of lap joints shows similar endurable load amplitudes. The critical location of failure is the intersection of the fused zone with the joint plane.

Keywords: Ultra-high strength steels; welding; fatigue; load capacity; heat treatment

1. Introduction

Considerations to improve resource efficiency have led to the use of stainless steels with a martensitic structure. These steels have advantages due to their inherent corrosion resistance, excellent formability and hardenability. The use of press-hardened steels can help to reduce the dead weight of components and/or

* Corresponding author.
E-mail address: martin.dahmen@ilt.fraunhofer.de.

significantly increase the payload of machines, vehicles, and conveyors. As the positive properties of components with welded joints using ultra-high strength steels are identified and validated, the range of applications will continue to expand. In this contribution selected results of a research project on dissimilar welding of ultra-high strength steels (Dahmen, Möller ,Olfert, 2021) will be presented.

2. Experimental

2.1. Materials

Materials under investigation comprise two high alloyed stainless grades and three low and un-alloyed steels. The investigations have been carried out on the following materials:

- Stainless chromium steel with martensitic-austenitic X46Cr13 (1.4034), press hardened to R_m = 1900 MPa, $R_{p0,2}$ = 1050 MPa, and tensile strain A_5 = 13%, with 0,9 and 1,2 mm thick;
- High manganese steel with austenitic microstructure X30MnCrN 16 14 (1.4678), cold rolled to R_m = 1200 MPa, $R_{p0,2}$ = 1000 MPa, and tensile strain A_5 = 13%, 1,2 mm thick;
- Martensitic manganese-boron steel 22 MnB5 1.5528 without coating, press hardened to R_m = 1500 MPa, $R_{p0,2}$ = 1350 MPa,
  and tensile strain A_5 = 10%, 1,5 mm thick;
- Dual-phase steel with ferritic-martensitic microstructure DP980 (1.0944), mechanical properties R_m = 1000 MPa, $R_{p0,2}$ = 760 MPa , and tensile strain A_5 = 14%, 1,5 mm thick;
- Micro-alloyed steel S500MC (1.0984), mechanical properties R_m = 600 MPa, $R_{p0,2}$ = 500 MPa, and tensile strain A_5 = 12%, 2 mm thick.

Table 1. Chemical compositions of the materials under investigation

	C	Si	Mn	S	P	Cr	Ni	N	B	Cu	Al	Ti	V
	m.%	m.%	m.%	m.%	m.%	m.%	m.%	m.%	ppm				
1.4034	0,47	0,33	0,72			12,76	0,32			0,11x			
1.5528	0,25	0,4	1,35	0,01	0,015	0,15			25				
1.4678	0,32					14	16	0,3		0,5			
1.0944	0,22	0,45	1,9	0,01	0,04						1,2		0.15
1.0984	0,1	0,42	1,4	0,01	0,02			0,05			0,04	0,09	0,14

Table 1 shows the chemical composition of the materials. For reference the combination 1.4034 was tested in similar welds. The combination takes 1.4034 as basis and the four other materials as dissimilar partner.

2.2. Welding and heat treatment

Most of the parameter development was carried out on a Cartesian robot. A Trumpf TRUDISK 12002) disk laser served as the beam source and an optical fibre cable with a 200 µm core diameter was used. For focusing, standard optics with a collimator focal length of f_K = 200 mm and a focusing focal length of f = 600 mm were used, so that a focus diameter of 607 µm was achieved. For the process development for welding the contour seams, a test rig was set up using a scanner. A fibre laser (IPG YLF 4000) with a maximum power of 4 kW was used as the beam source. The beam was guided via a fibre with a core diameter of 100 µm. With a collimator focal length of f_K = 100 mm and a focusing focal length of the plane field lens of f = 330 mm, a beam diameter of 320 mm was achieved at the focus.

The heat treatment was carried out as tempering in a convection oven applying a temperature range from 300 to 700°C. Heating rates between 1.7 and 3.4 K/s were achieved. A KS2 sample with drag element was used to record the temperature. The cooling rates varied with the type of cooling medium. When cooling in still air, the cooling rate was 1.5 to 3 K/s, with gas cooling between 34 and 65 K/s and with quenching in water about 100 K/s.

The welds were initially tested by Vickers hardness test and by shear tensile tests at overlap joints to obtain information about the distribution of mechanical properties over the weld zone as well al the nature of fracture.

2.3. Testing load capacity

The LWF-KS2 specimen (Hahn, Kurzok and Oefer, 1999 and EFB/DVS, 2007) was used to investigate and evaluate the load-capacity and failure behavior with different load application angles. With the specimen geometry, load application angles of 0°, a pure shear tensile load, 30°, 60° and 90°, a pure head tensile load, were realized. The LWF-KS-2 specimen developed at the LWF is used to determine connection characteristics of point, surface and linear joining elements under quasi-static, impact and cyclic loading.

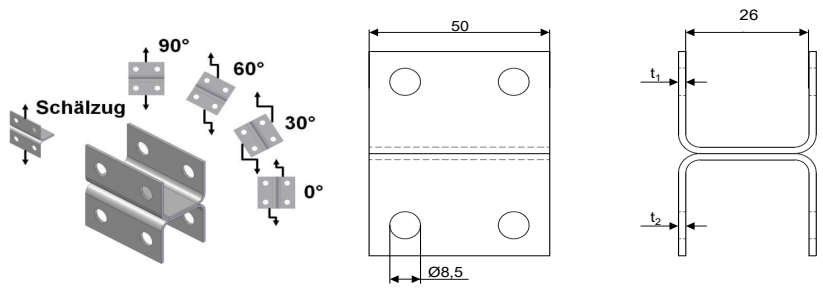

Fig. 1. View and drawing of a KS-2 specimen

Due to the specimen geometry, combinations of the load types head tension and shear tension can also be made possible. The LWF-KS2 specimen consists of two symmetrical U-profiles manufactured by forming technology. The two profiles are joined on the flat surface by means of a joining process. In this case, the LWF-KS-2 specimen is only provided with one leg. The geometry and load types of the LWF-KS2 specimen used are shown in Figure 1.

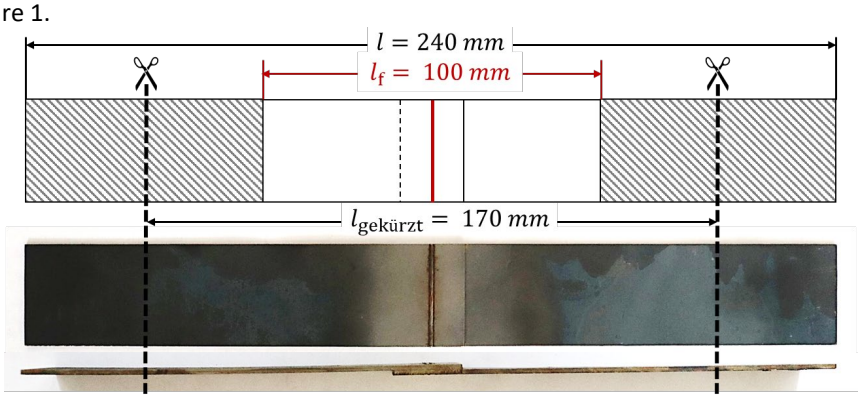

Fig. 2. Specimen for the fatigue test of lap welds. The dashed lines show the shortened specimen for highly distorted specimens.

Besides of the angles the deformation speed was varied during the KS2 tests. In the first case, the quasi-static loading, was carried out under deformation rate of 10 mm/min. For the second case, dynamic or crash loading, a deformation rate of 2 m/s was applied. A GOM Aramis system was used to evaluate the deformation behavior in the immediate vicinity of the examined weld seam.

2.4. Fatigue testing

For the experimental investigation in force-controlled cyclic tests, straight specimens of length l = 240 mm without tapering are taken from the laser welded sheets according to figure 2. For the cyclic testing of these laser welds with root failure, the quality of the laser-cut side surfaces is sufficient, especially for line and clamp welds with weld start/end. The influence of the laser cut edge on the fatigue strength is at least negligible, for samples with seam beginning and end anyway irrelevant to failure. The clamping area in the test setup is 70 mm in length and 30 mm in width specimen width per specimen half (shaded area in Figure 2). This results in a free clamping length (test length) of 100 mm.

To derive force Wöhler curves and as a basis for the loading ability in the notch stress system, force-controlled cyclic tests are carried out with the servo-hydraulically operated test system. The force is transmitted from a hydraulic cylinder via a flat specimen clamp to the examined laser beam welded overlap specimens of the geometry documented in Figure 2. The tests are carried out at a load ratio of $R_F = 0$ with a tensile swell. The sinusoidally applied test forces are controlled in the test by a force transducer. The test frequency is usually f = 30 Hz and is only increased to 40 Hz at the beginning of the test for very low load amplitudes, e.g. for run-through tests.

3. Results

3.1. Welding metallurgy and strength

Figure 3 shows the results of the shear tensile tests dependent on the heat treatment parameters temperature, soaking time, and cooling conditions. The force at fracture becomes maximum at a temperature of 400°C and minimum at 700°C. This coincides with the fact that full tempering is achieved in the temperature range between 670 and 780°C. At low temperatures up to 300°C the strength values show a large scattering. the reason for this is the limited effect of heat treatment in this temperature range. The structure of the weld zone showing high hardness peaks due to the formation of un-tempered martensite remains unchanged. A large amount of brittle fracture at the fusion line is the consequence.

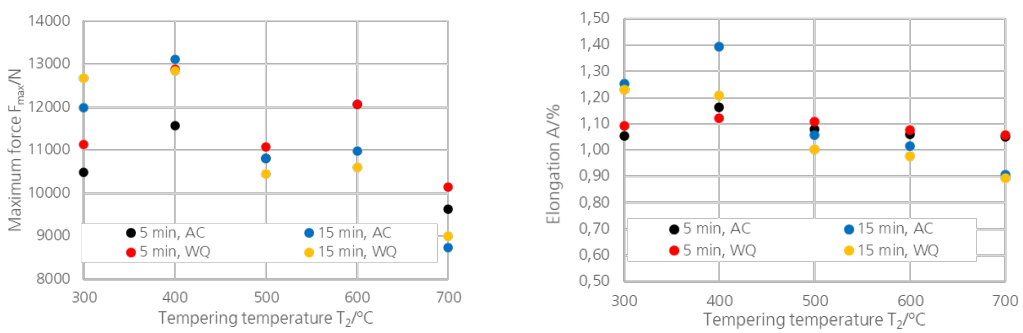

a) Breaking force b) Elongation at fracture

Fig. 3. Shear strength and relative displacement dependent on the tempering temperature

As the optimum temperature for post-weld heat treatment 400°C was identified. In figure 4 cross-sectional views of the fracture as well as images of the fracture surfaces are shown. The parameters soaking time and cooling condition were varied. After heating for 5 min followed by water quenching fracture is introduced at a distance from 0 to 1.2 mm from the fusion line at their section with the joint plane. The course of the crack deviates into the softer zones where the material is tempered by the welding heat. Specifically, at this parameter frequent failure at the central region of the sheet was observed. This effect was not seen if the soaking time was set to 15 minutes (figure 4b). In this case fracture starts within a range or 0.4 mm from the fusion line. Origin is again the intersection of fusion line and fusion plane.

The fractographic inspection revealed the origin of the fracture and its general nature. Figure 4c shows in the upper part a low-magnification image of the crack surface of a specimen heated for 5 min followed by air cooling. The origin of fracture is seen as a small indentation at the lower boundary of the sheet. In higher magnification the fracture surface shows a predominant ductile behaviour with only single indication of cleavage at grain boundaries. The crack surface of a specimen tempered for 15 min followed by water quenching shows a radiant initiation of the fracture at the lower sheet boundary. In high magnification the crack surface appears predominantly ductile but show also numerous carbide particles in the dimples. Obviously, the fracture follows a line with pronounce carbide precipitation.

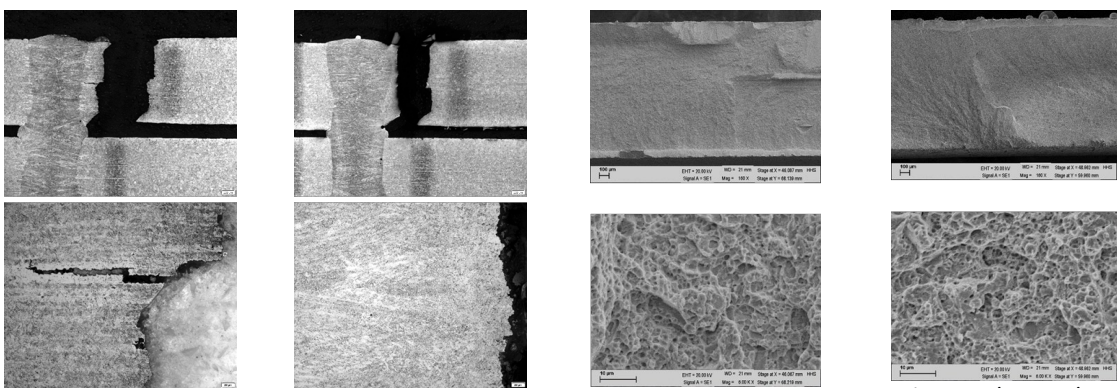

a) 400°C/5 min/WQ b) 400°C/15 min/WQ c) 400°C/5 min/AC d) 400°C/15min/WQ

Fig. 4. Fracture location and surface of shear tensile specimens heated at different soaking time and varying cooling conditions.

Based on these findings the optimum temperature for post-weld heat treatment was set to 400°C. The longer dwell time provided by air cooling seems to lead to a more ductile behaviour of the fracture.

3.2. Load capacity

In first preliminary tests all material combinations were teste das welded under quasi-static conditions. Maximum forces range between approximately 13 kN for shear load (load angle 0°) to 1 kN for cross tensile load. The deformation amounts to 0.4 to 2.1 mm respectively. A strong cross tensile sensitivity of the connection is clearly visible. Under pure shear tensile load, the joint exhibits the greatest load capacity and deformation behaviour. When a cross-tensile force component occurs, the maximum force and the deformation at fracture decrease strongly. The load capacity remains almost at the same level and shows no significant at varying load angles between 30 and 90°.

The fracture patterns of the quasi-static tests under 0° load direction show fracture surfaces that exhibit a shear fracture in the plane of the joint between the sheets. The uniformly brittle shear fracture at the dendrite

boundary is due to the mechanical load. Pre-existing weld failures as porosity and micro cracks are assumed to be the reason for low forces and high scattering.

Figure 5 shows a comparison of the KS2 test results on welds which underwent a post-weld heat treatment. The load capacity could be significantly increased for almost all material combinations. Only in the combination with the 1.4678 there is deviation from the common pattern. in this case the load-bearing capacity of the 0° specimens was reduced by 24 % through the post-weld heat treatment. The cross tensile sensitivity could be significantly reduced for all tested material combinations. The load-bearing capacity of the intermediate angles 30° and 60° is higher than under pure head tensile loading at 90° loading. The post-weld heat treatment has shown greatest effect on the 90° specimens of material combination with the manganese-boron steel 1.5528 with a 415 % increase in maximum force.

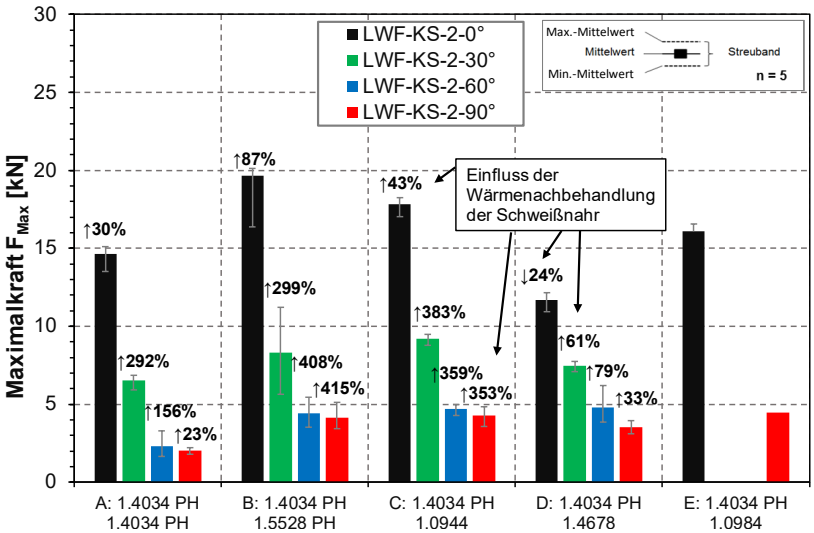

Fig. 5. Comparison of the maximum forces of all material combination as line welds after post heat treatment at 400°C/5 min/AC) under quasi-static loading

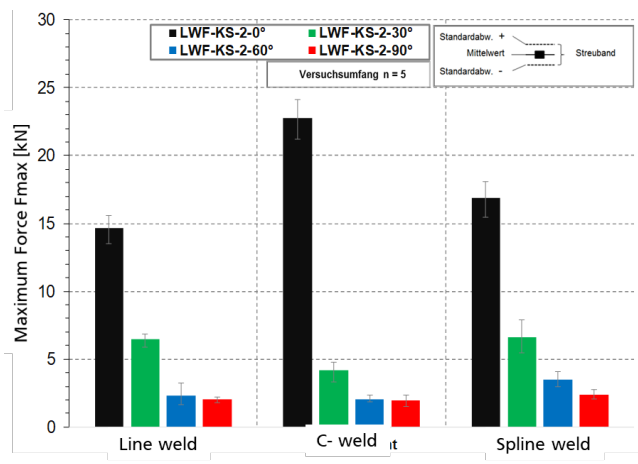

Fig. 6. Comparison of the maximum forces of the material combination A under variation of the weld geometry (heat treatment 400°C) under quasi-static loading

The bar graphs in figure 6 show a comparison of the average maximum forces for different weld contours attained in the quasistatic KS2 test at similar welds of press hardened 1.4034. Shear forces are minimum for the line welds if loaded in longitudinal direction. Spline welds show a little greater load capacity under the same load direction. Obviously the apparently wider seam contributes to this effect. If a cross-tensile component appears the load capacity shows an identical behaviour in both cases. Highest load capacity is achieved in the C-welds when loaded under 0° (shear) along the short axis of the contour whereas load capacity becomes minimum if a cross-tensile component occurs. Especially at angles 60 and 90° C-welds are comparable to line welds. Strong notch effects are assumed to be a reason for the early failure in C and line welds.

As a tendency, it can be deduced from the results that the change of the seam geometry from line seam to clamp seam has a negative effect on the head tension load capacity. The load-bearing capacity of the load angles with cross tension component decreases for all material combinations. The maximum load-bearing capacity under pure shear tensile load, on the other hand, has increased by 55% for the similar welds and did not change significantly for the other material combinations examined where an increase in load capacity of only up to 8% was observed. The spline seam, on the other hand, has no significant influence on the load-bearing capacity of the LWF-KS-2 specimens.

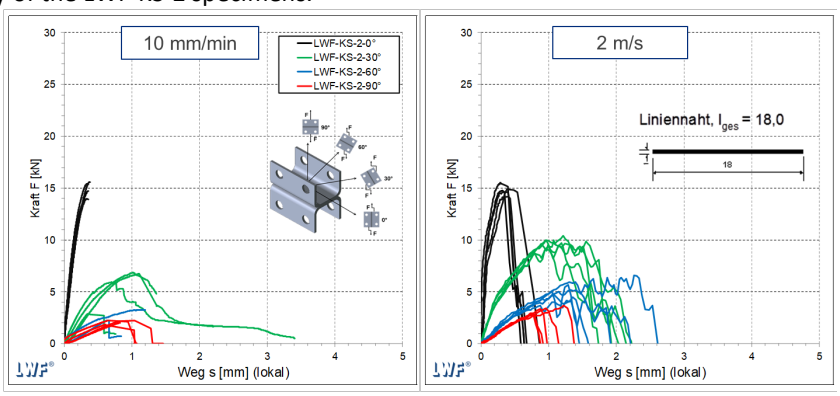

Fig. 7. Force displacement curves for the similar lap welds in 1.4034 under quasi-static and impact load

In figure 7 force-displacement diagrams for the quasi-static regime at 10 mm/min and the dynamic regime at 2 m/s are displayed. As seam contour the line weld of 18 mm length is considered. As the most critical joint the similar weld of 1.4034 was used for the representation. The maximum forces vary in a range of 2.9 kN and 15.5 kN. The curves under 0° loading show comparable stiffness, maximum force and elongation at break. With the occurrence or the cross-tensile component in the load the specimens tested dynamically show significantly higher maximum forces compared to the quasi-static tests. Specimens with a C-weld show a very high scattering in the maximum forces as well as in the elongation at break. Therefor the effect of the deformation is difficult to assess. Test at spline welds show the same results as for straight welds except with a 20% increase in maximum force under shear load.

3.3. Fatigue test results and cyclic material behavior

The starting point for characterising the cyclic material behaviour is the evaluation of strain-controlled, cyclic tests at different total strain amplitudes. In the frame of strain-controlled tests firstly the cyclic material properties in un-welded state were established. Figure 7a shows a cyclic stress-strain curve for the material. 1.4678, grade H1000, loaded in the directions parallel to the rolling texture.

From the cyclic stress-strain curves of the respective materials, the cyclic yield strengths $R'_{p0.2}$ can be derived. Figure 7b compares the cyclic yield strengths characteristic for the cyclic stress-strain curves according to compatibility with the tri-linear strain-approximation curve of the materials investigated. For the 1.4034 PH, the highest cyclic strength results with $R'_{p0.2} \approx 1200$ MPa. The also press-hardened 1.5528 follows with $R'_{p0.2} = 1062$ MPa. Lower values result for the 1.0944 ($R'_{p0,2} = 570$ MPa) and 1.0984 ($R'_{p0,2} = 508$ MPa). For the different material states of 1.4678, the cyclic strength increases with increasing material strength from $R'_{p0.2} \approx 450$ MPa (H500) to $R'_{p0.2} = 930$ MPa and $R'_{p0.2} = 952$ MPa (H1000, transverse to the rolling direction). The materials in this study thus have significantly different cyclic strengths, the effects of which were to be investigated in the welded state.

The test results of the lap welded specimens for all material combinations, i.e. laser beam welded of the similar and dissimilar types, as well as for all three seam types, i.e. continuous line weld, stitched line weld and C-weld, are plotted in the Wöhler diagram in figure 8. The load amplitudes applied in the cyclic test with the load ratio of $R_F = 0$ are compared to the number of cycles to failure. The experimental results are by a Wöhler line evaluated based on the Maximum Likelihood Estimation (MLE).

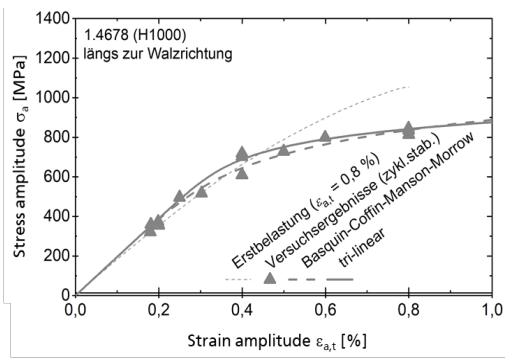

a) Cyclic stress-strain curve of 1.4678 (H1000)

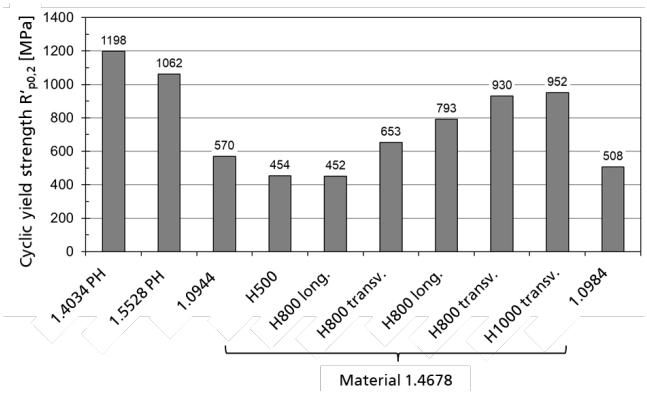

b) Cyclic yield strengths *R'*$_{p0.2}$ of investigated materials

Fig. 7. Cyclic mechanical properties of the materials under investigation

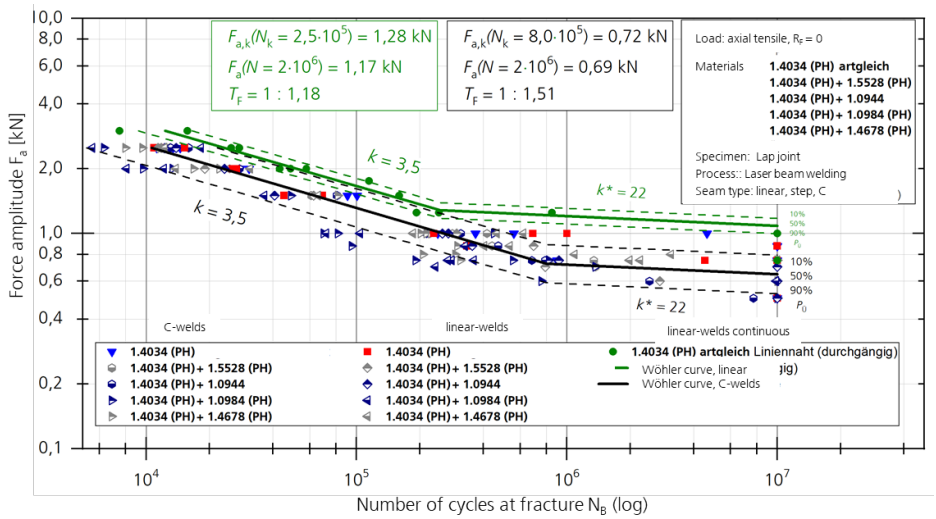

Fig. 8. Load-based Wöhler test results of lap joints

In a first step the seam types will be separately assessed by MLE. A comparison of both Wöhler curves delivers almost no difference between the two curves with respect to increased force amplitudes in the range of fatigue strength at a force amplitude $F_a \geq 1{,}5$ kN. The slopes differ only slightly with an slope of $k = 3{,}6$ for welds with 18 m length and $k = 3{,}4$ for C welds. There is also only little difference in the force amplitudes at the transition point ($N_k = 8{,}0 \cdot 10^5$) and hence, the force amplitudes at number of cycles $N = 2{,}0 \cdot 10^6$ at a likelihood of 50% amount to:

- Line weld 18 mm: $F_{a,k}(N_k = 8{,}0 \cdot 10^5) = 0{,}75$ kN and $F_a(N = 2{,}0 \cdot 10^6) = 0{,}72$ kN,
- C-weld: $F_{a,k}(N_k = 8{,}0 \cdot 10^5) = 0{,}70$ kN and $F_a(N = 2{,}0 \cdot 10^6) = 0{,}67$ kN.

Under axial cyclic load there is thus a factor of approximately 1.07 between laser beam welded line stitch and C-welds of the material combinations examined. For the application in cyclically loaded components, it must therefore be examined whether the slightly higher fatigue strength of the line stitch welds in the range of longer lifetimes of a number of cycles greater than $1.0\text{-}10^5$ is outweighed by a potentially higher fatigue strength of the C-clamp welds in the application-related load case, such as other load angles in the sheet plane, or even moves into the background. Furthermore, the scatter of in the line welds of 18 mm length of 1 : 1.49 in the C-welds 1 : 1.52 is almost identical, so that the results described above can also be transferred to other survival probabilities.

4. Discussion

Joining of dissimilar joints was investigated by varying the parameters focal diameter and welding speed. In general, the melt was found to be poorly mixed, resulting in a highly zoned structure of the welds. In connection with the high manganese steel, a predominantly austenitic structure is present, which causes low strengths. In the joints, a mixed structure of martensite and bainite is present. The fluctuation of the local strengths, represented by the Vickers hardness, is very pronounced in these compounds. This, in combination with an increased hardness at the fusion line and tempering in the heat-affected zone, especially in the case of manganese-boron steels and dual-phase steels, leads to strong notch effects, which negatively influence the strengths of the compound.

A post heat treatment of dissimilar joints with unalloyed and low-alloyed steels can lead to an improvement of the results with respect to homogenization of the hardness profile. There are narrow limits to this, especially with respect to tempering temperatures. While the tempering limit for the material 1.4034 is about 550°C, this critical temperature for the dual-phase steels has a value between 400 and 500°C, depending on the carbon and martensite content. The press-hardened manganese-boron steels lose their strength already at temperatures of 300°C. For these joints, the heat control must be carefully matched to the material combination.

Connections with the high manganese steel 1.4678 represent a special case in the investigation. The tempering stability of grade H1000 up to a temperature of 800°C could not be confirmed in the welded joints, as a steady transition of the hardness from the weld (350 HV0.2) to the level in the base metal (500 HV0.2) was measured in the heat-affected zone. The hardness cannot be influenced by heat treatment. To increase hardness and thus the strength of the joint here, alloying measures (filler material) or mechanical treatment can be considered. This can be the subject of future investigations.

The heat treatment during welding must be adapted to the production of cubic martensite. Increasing the temperature alone is not sufficient, and long holding times should be avoided, as this leads to increased carbide precipitation. The result is a strong inhomogeneity of the microstructure in the coarse grain zone directly at the fusion line. Suitable heat management should include preheating. In conjunction with this, annealing can be carried out from the welding heat, which can reduce the cooling rates. This both improves

the toughness of the joint and prevents the formation of cold cracks in the joining process, which occurred especially in the dissimilar joint with unalloyed grades.

The load capacity was determined on I-seams at the lap joint. For non-heat-treated specimens, the maximum load was achieved under pure shear tensile loading. When a head tensile force occurs, the maximum force decreases strongly and depends only to a small extent on the load application angle. The results vary greatly, especially with respect to the fracture path. The ultimate loads can be increased by post heat treatment, except for the combination with the high manganese steel 1.4678. The smallest increases are found for the high manganese steel. The smallest increases are achieved in the same type of combination with 1.4034. With the other combinations, it could be increased significantly. The head tensile strength could also be significantly reduced. The seam contour at the transition from the line weld to the clamp weld led to a reduction in the load-bearing capacity, which decreases for all material combinations at load angles with a head tensile component. The spline seam, on the other hand, has no significant influence on the load capacity of the LWF-KS-2 specimens. The layer sequence of the sheets, which describes which material is positioned on the side facing the beam, has a major influence on the load-bearing capacity. While the load-bearing capacity could be increased in the combination with the steel 1.4678, especially at load angles with head tension, a reduction was found in the combinations with unalloyed and low-alloyed steels. When testing the face welds, a very large drop in strength was found when a head tension component occurred. This is attributed to the modified specimen being more sensitive to slippage and tilting. This subsequently leads to a multi-axial stress state, which is also confirmed by a large scatter. The position of the seam transverse to the load direction also seems to have an influence. Despite the guidance, the specimen splayed open in the test, so that a considerable notch effect occurs in conjunction with transverse bending.

The evaluation of the fatigue strength comprises on the one hand the characterisation of the cyclic material behaviour and on the other hand the concept-related fatigue strength evaluation of the welded joints in the load, nominal stress and notch stress system. The analysis of the cyclic material behaviour highlights the very different cyclic properties of the investigated base materials, such as a particularly high cyclic $R'_{p0.2}$ yield strength of approx. 1200 MPa for the press-hardened 1.4034. The tri-linear strain-elongation curve and the cyclic stress-strain curve derived from it, taking into account the compatibility conditions, represent the results very well. The press hardened 1.4034 butt joint of the same type can also be characterised regarding its cyclic behaviour on the basis of strain-controlled vibration tests and associated characteristic values can be derived. On the basis of the press hardened 1.4034 reference material, laser beam welded lap joints of the same and different types with line and clamp welds were experimentally characterised and compared in load-based tests. The cyclic failure originates from the sharp notches in the joint plane between the sheet overlap. If the results for line stitch and C-welds are separated from those of continuous line welds, the evaluation of the former across the test series results in the lowest scatter of the investigated evaluation approaches of T = 1 : 1.51 as a result of the force camber line. Dissimilar lap joints consistently show a lower fatigue strength than similar ones in $2 \cdot 10^6$ cycles. Based on the nominal stress definition for the load-transmitting seam cross-section, a conservative design by FAT 36 follows from the nominal stress evaluation, which is applied in the IIW recommendations for lap joints with fillet welds on both sides and seam root failure. The notch stress evaluation taking into account sheet thicknesses and seam width in the FE modelling provides a mostly conservative evaluation compared to FAT 630 with the slope of k = 5, but with a larger scatter of results. This can be explained by a different recording of influences, such as seam dimensions in the nominal stress concept or excess stresses in the notch stress concept, depending on the evaluation concept. By considering the maximum stressed length of the weld in the evaluation, this scatter is reduced to T = 1 : 1.86 for tolerable modified notch stresses.

5. Conclusions

Results of welding and mechanical testing of similar and dissimilar joints on the base of a press-hardened chromium steel have been presented. The high carbon content of the chromium steel needs weld heat treatment in order to be welded maintaining high strength and ductility. With respect to the joining partners a post-weld heat treatment at 400°C was advantageous proven in LWF-KS2 tests and fatigue tests.

An effect of the seam contour could not have been derived. In KS-tests as well as in fatigue testing only small differences on the strength were measured. As major reasons for this effect notch effects caused by inhomogeneous distribution of local mechanical properties (hardness), metallurgy, and peaks in residual stresses are assumed. Further experimental investigations and investigations will show to which degree these features contribute to the strength and ductility of joints using ultra-high strength steels.

Acknowledgements

The research project IFG 19556 N / FOSTA-P-1175 "Weiterentwicklung, fügetechnische Absicherung und technische Auslegung von Schweißverbindungen mit martensitischen Chromstählen" from the Research Association for steel Application (FOSTA), Düsseldorf, was supported by the Federal Ministry of Economic Affairs and Energy through the German Federation of Industrial Research Associations (AiF) as part of the programme for promoting industrial cooperative research (IGF) on the basis of a decision by the German Bundestag. The project was carried out at Fraunhofer Institute for Laser Technology, Research group System Reliability, Adaptive Structures, and Machine Acoustics of Darmstadt Technical University, and Laboratory for Material and Joining Technology of Paderborn University.

References

Dahmen, M, Möller, B, Olfert, V, 2021. Weiterentwicklung, fügetechnische Absicherung und technische Auslegung von Schweißverbindungen mit martensitischen Chromstählen. Final Repoprt on FOSTA Project P 1175, under preparation.

Hahn, O., Kurzok, J.R., Oefer, M., 1999. Prüfvorschrift für die LWF KS2-Probe. Laboratorium für Werkstoff- und Fügetechnik (LWF), Paderborn University

EFB/DVS-Merkblatt 3840 (12/2007), 2007. Prüfung von Verbindungseigenschaften – Prüfung der Eigenschaften mechanisch und kombiniert mittels Kleben gefertigter Verbindungen. Düsseldorf